nature geoscience

LETTERS

PUBLISHED ONLINE: 18 JULY 2016 | DOI: 10.1038/NGEO2770

The tropical Pacific as a key pacemaker of the variable rates of global warming

Yu Kosaka[1]* and Shang-Ping Xie[2]*

Global mean surface temperature change over the past 120 years resembles a rising staircase[1,2]: the overall warming trend was interrupted by the mid-twentieth-century big hiatus and the warming slowdown[2–8] since about 1998. The Interdecadal Pacific Oscillation[9,10] has been implicated in modulations of global mean surface temperatures[6,11], but which part of the mode drives the variability in warming rates is unclear. Here we present a successful simulation of the global warming staircase since 1900 with a global ocean–atmosphere coupled model where tropical Pacific sea surface temperatures are forced to follow the observed evolution. Without prescribed tropical Pacific variability, the same model, on average, produces a continual warming trend that accelerates after the 1960s. We identify four events where the tropical Pacific decadal cooling markedly slowed down the warming trend. Matching the observed spatial and seasonal fingerprints we identify the tropical Pacific as a key pacemaker of the warming staircase, with radiative forcing driving the overall warming trend. Specifically, tropical Pacific variability amplifies the first warming epoch of the 1910s–1940s and determines the timing when the big hiatus starts and ends. Our method of removing internal variability from the observed record can be used for real-time monitoring of anthropogenic warming.

Global mean surface temperature (GMST) has increased since the nineteenth century by nearly 1 °C. The observed warming is not monotonic but accompanied by notable interdecadal modulations, forming the global warming 'staircase'[1,2] (Fig. 1a). The last step of this staircase is the surface warming slowdown since 1998[2–8,12]. The recent rate of GMST increase is much smaller than during the 1970s–1990s even though the radiative forcing is comparable between the two epochs[2,12]. Indeed it is smaller than the ensemble average of model simulations forced by radiative forcing[12] (Supplementary Fig. 1). The transition of the Interdecadal Pacific Oscillation (IPO)[9,10] from a positive to negative state is the leading mechanism for the recent slowdown[3,6], as corroborated by pacemaker experiments using coupled climate models[4,5]. Additional contributions come from volcanic and other radiative forcing[7,8].

The first warming epoch of the rising staircase started around 1910 and lasted until the 1940s, with a rate comparable to the 1970s–1990s (Fig. 1a) despite much weaker radiative forcing. The warming was interrupted by the big hiatus for the 1940s–1970s, followed by the second warming epoch until the 1990s and the recent warming slowdown. While the global IPO mode has been suggested to drive internal modulations of GMST[6,11,13] (Supplementary Fig. 2), we use a partially coupled experiment[4] to narrow the pacemaker to the tropical Pacific. Compared with previous studies, our experiment allows for year-by-year validation against observations, and accommodates variations in the tropical Pacific SST pattern between interannual and decadal timescales, and among IPO events.

We use two experiments with a global ocean–atmosphere coupled model starting in the late nineteenth century, forced with common radiative forcing (Methods). In one experiment (HIST), internal climate variability evolves freely, and averaging across a 20-member initial-condition ensemble isolates the forced response. In a Pacific Ocean–Global Atmosphere (POGA) pacemaker experiment, we restored sea surface temperature (SST) anomalies in the equatorial Eastern Pacific to follow the observed history[14].

In HIST, GMST (T_{HIST}) shows piecewise linear warming interrupted by volcanic eruptions (Fig. 1a; also Supplementary Fig. 1). A quasi-linear warming epoch begins in the 1900s and continues until the 1960s. After the 1963 eruption of Agung, GMST rises faster, interrupted by 1982 El Chichón and 1991 Pinatubo eruptions. POGA (T_{POGA}) reproduces the observed (T_{obs}) staircase-like warming quite well (Fig. 1a). The twentieth-century warming is concentrated in two epochs from around 1910 to the 1940s and from the 1970s to 1990s, intervened by the big hiatus as observed (Fig. 1a,b). POGA's skill in annual GMST extends through the 135 years with high correlation with observations (Supplementary Table 1). Compared to sharp GMST drops in HIST ensemble mean, volcanic signals are indistinguishable from other interannual variability in observations and POGA.

Constraining tropical Pacific variability in POGA reduces inter-member variance of GMST by 68%, indicating the dominant role of the IPO and El Niño–Southern Oscillation (ENSO) in internal GMST variability. Despite the small area of SST restoration (<10% of the Earth's surface), a 1 °C increase in tropical Pacific SST raises GMST by 0.33 °C, and this tropical Pacific effect is more pronounced on the decadal than interannual timescale (Supplementary Fig. 3). Namely, the IPO is more influential on GMST than ENSO. The timescale dependence highlights the advantage of dynamical models over empirical methods that are based on interannual ENSO and underestimate the IPO effect[6–8].

Major discrepancies between POGA and observations are found in the 1880s to early 1890s and around World War II (Fig. 1a). The former is likely to be due to overestimation of radiative forcing by the 1883 Krakatau eruption (as evident in T_{HIST}) or observational errors. During World War II, interannual correlation between GMST and tropical Pacific SST drops in observations but not in the model (Supplementary Fig. 4), suggesting large observational errors in either GMST[15] or tropical Pacific SST. Indeed for 1942–1946, the tropical Pacific SST in Extended Reconstructed SST (ERSST) version 3b (ref. 14) used for POGA is biased low by 0.07–0.08 °C compared with newer data sets of ERSST version 4 (ref. 16) and Hadley Centre Ice-SST version 2.1, explaining roughly 20% of the GMST bias. The rest may be due to Arctic warming in the 1930s[17],

[1]Research Center for Advanced Science and Technology, University of Tokyo, 4-6-1 Komaba, Meguro-ku, Tokyo 153-8904, Japan. [2]Scripps Institution of Oceanography, University of California San Diego, 9500 Gilman Drive MC 0206, La Jolla, California 92093, USA.
*e-mail: ykosaka@atmos.rcast.u-tokyo.ac.jp; sxie@ucsd.edu

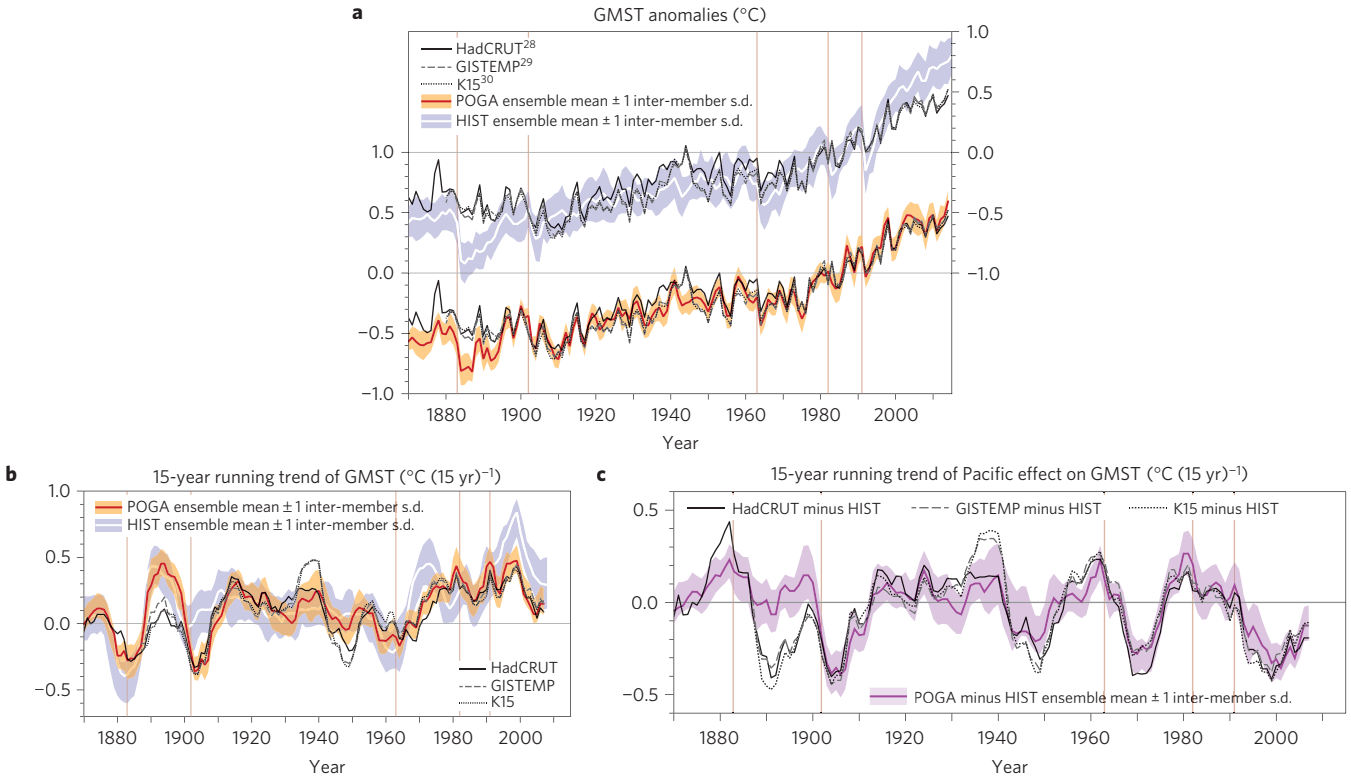

Figure 1 | Annual GMST and its trend. a, Observed[28–30] and simulated GMST anomalies. HIST and POGA (right and left axes, respectively) are offset by 1 °C, along with observations. Anomalies are relative to 1970–1999 averages for observations and POGA, and to the POGA average for HIST. **b**,**c**, Running 15-year trend of GMST in HIST, POGA and observations (**b**) and for the tropical Pacific effect (POGA minus HIST and observations minus HIST) (**c**). The trend is plotted at year 8 of the 15-year window. Brown vertical lines indicate major volcanic eruptions in the tropics.

which is underestimated in POGA (Supplementary Fig. 5). Indeed the second mode of internal decadal GMST variability after the IPO shows a large loading around the Arctic (Supplementary Fig. 6). The tropical Pacific effect on the Arctic mode is weak.

Subtracting the HIST ensemble mean from POGA isolates the influence of tropical Pacific internal variability. The tropical Pacific effect ($T_{POGA} - T_{HIST}$) is comparable to radiative forcing on decadal GMST changes (Fig. 1c purple versus Fig. 1b white curves). There were four major cooling events due to tropical Pacific variability in the past 120 years—in the 1900s, 1940s, around 1970 and 2000 (Fig. 1c). (We exclude the event around 1890 because of forcing and data uncertainty.) The tropical Pacific started cooling in the early 1990s[5], offsetting the acceleration of GMST increase in a recovery from the 1991 Pinatubo eruption (the peak around 2000 in HIST GMST tendency) (Fig. 1b). Afterwards, the tropical Pacific effect became comparable with the radiative forcing, causing the recent warming slowdown. While the mid-twentieth-century big hiatus has been loosely attributed to anthropogenic aerosol increase[18,19], two tropical Pacific cooling events during the 1940s and 1970s mark the beginning and end of the hiatus epoch. The latter event prolonged the big hiatus until the mid-1970s[20], which would otherwise have ended in the 1960s (Fig. 1a,b and Supplementary Fig. 1). Further back in time, there was a decadal GMST decrease around the turn of the twentieth century attributable mostly to tropical Pacific cooling (Fig. 1b,c). Between these cooling/slowdown events were accelerations of GMST increase due to the tropical Pacific warming (Fig. 1c and Supplementary Table 2) superimposed on positive radiative forcing. Tropical Pacific variability contributed to the rapid warming from the 1910s to 1930s, substantiating a geochemical proxy study[21]. Thus, tropical Pacific variability determined the timing of transitions between warming acceleration and slowdown epochs.

Beyond the global mean, we exploit spatial information for IPO fingerprints. We perform an empirical orthogonal function (EOF) analysis of 15-year trend of gridded annual mean $T_{POGA} - T_{HIST}$ and $T_{obs} - T_{HIST}$ in a domain spanning the tropics, subtropics, North Pacific and North America, excluding the region of SST restoring in POGA (Methods). The leading patterns are strikingly similar between the model and observations, with minor teleconnection biases including displaced anomalies in North America (Fig. 2a,b and Supplementary Fig. 7a). The corresponding time series are highly correlated between POGA and observations (Fig. 2c), featuring the four strong negative events noted earlier in GMST. POGA shows skills over the entire tropical and subtropical oceans and the North Pacific, and over land regions of India, Australia and North America, consistent with remote influence of tropical Pacific SST. POGA matches observed patterns of temperature anomalies well for all major events of GMST modulations, much better than HIST (Fig. 2d–i and Supplementary Fig. 8). POGA's skill is low over the North Atlantic and northern Eurasia where internal variability other than the IPO is important (Supplementary Fig. 6).

We further unpack the temperature trends to include the seasonal dimension by performing seasonal EOF analysis for the internal components of 15-year trends of zonal mean surface temperature. The IPO dominates the leading principal component in both observations and the model (Fig. 3d). Despite weak seasonality in the tropics, the IPO influence at northern high latitudes features a pronounced peak in late winter (Fig. 3a,b and Supplementary Fig. 7b). This results in a winter peak in GMST response to the IPO (Fig. 3c), consistent with the recent warming slowdown featuring strong GMST cooling in boreal winter and weak warming in summer[4].

Climate models were subjected to close scrutiny for the apparent failure to simulate the recent warming slowdown. Similar apparent

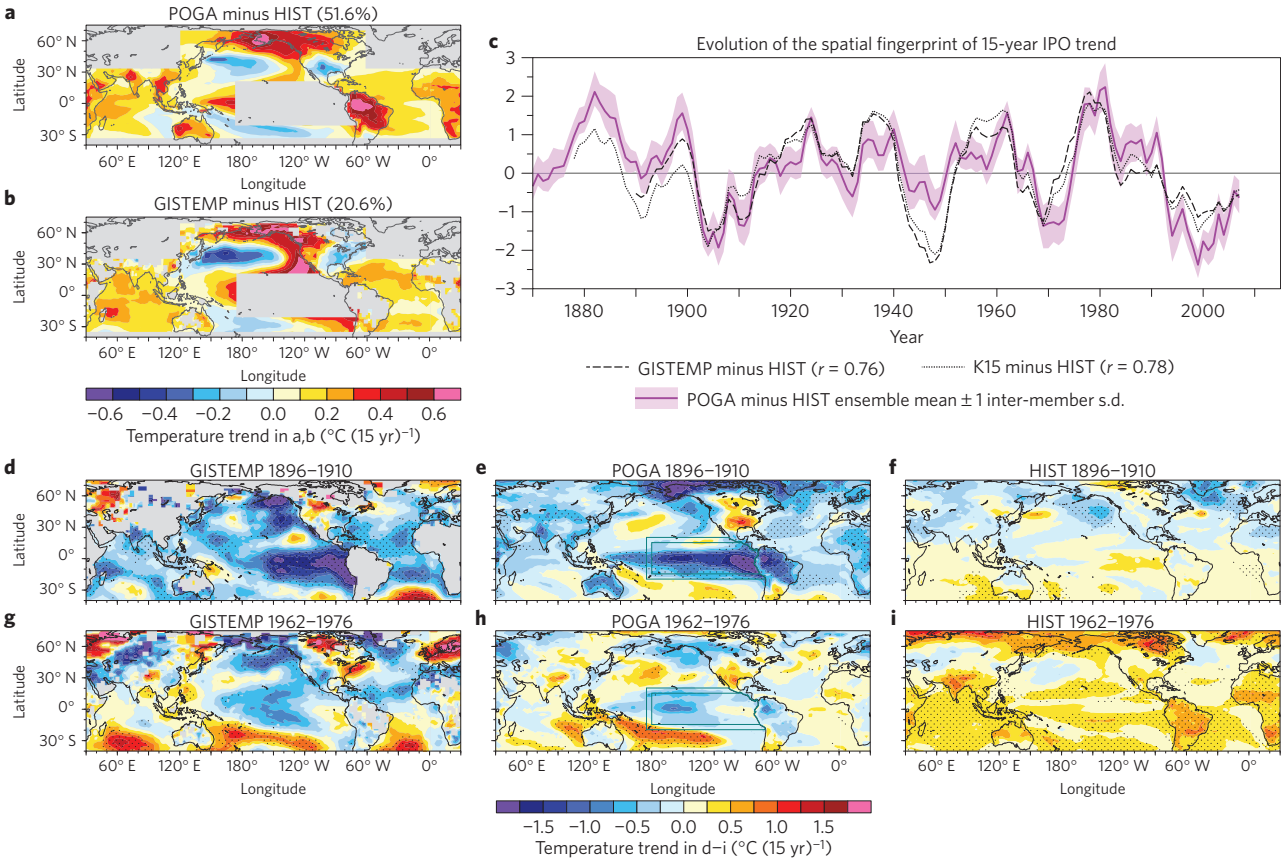

Figure 2 | A spatial fingerprint of the IPO. a,b, The leading EOF modes of 15-year annual mean surface temperature trends in POGA minus HIST (**a**) and observations minus HIST (**b**). **c**, The principal component time series. Correlation coefficients (*r*) with POGA minus HIST ensemble mean are indicated in the legend. **d–i**, Examples of annual mean surface temperature trends for IPO cooling events. GISTEMP (left), POGA (middle) and HIST (right) for 1896–1910 (**d–f**) and 1962–1976 (**g–i**). Stippling indicates trends that exceed the 95% confidence level on the basis of the Mann–Kendall test. Green boxes represent SST restoring region in POGA.

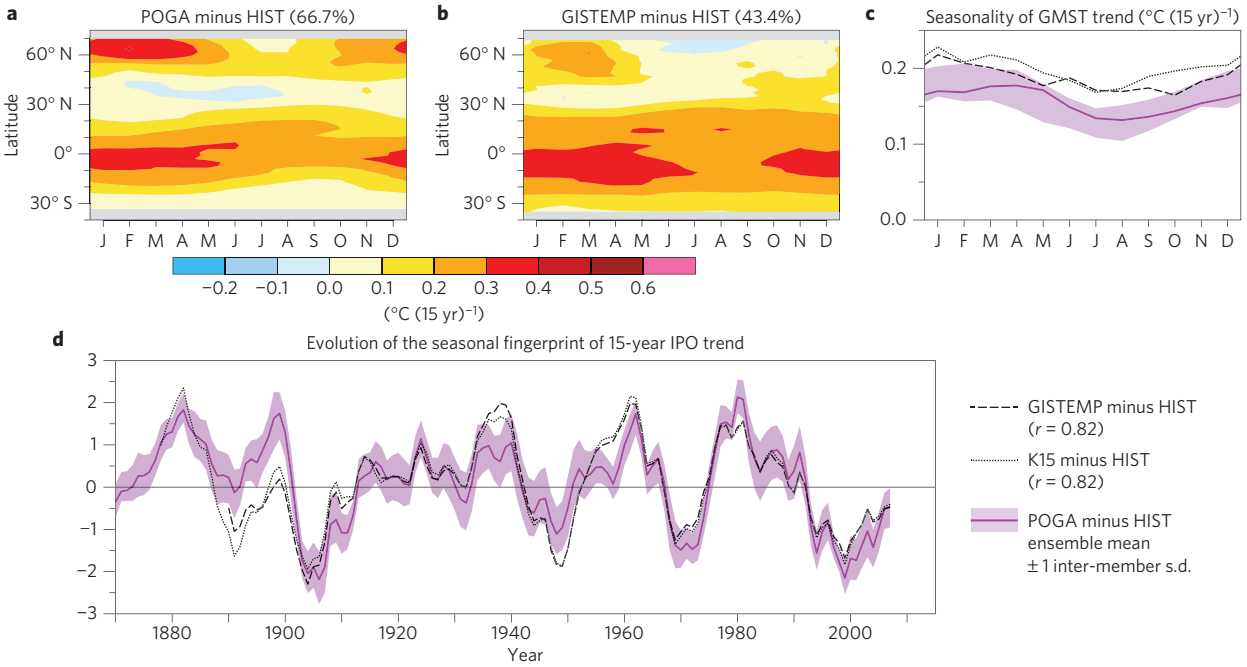

Figure 3 | A seasonal fingerprint of the IPO. The leading modes of seasonal EOF for 15-year trend of zonally averaged surface temperature over (35° S–70° N) of POGA minus HIST and observations minus HIST. **a,b**, Latitude–season patterns for POGA minus HIST (**a**) and observations minus HIST (**b**). **c**, Fifteen-year trend anomalies of seasonal mean GMST regressed against unit s.d. of the leading principal components. **d**, The leading principal component time series. Correlation coefficients (*r*) with POGA minus HIST ensemble mean are indicated in the legend.

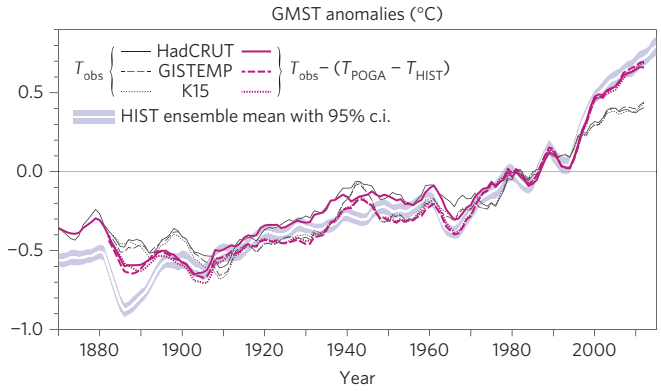

Figure 4 | Estimates of forced GMST anomalies. Five-year running mean anomalies (°C) of $T_{obs} - (T_{POGA} - T_{HIST})$ (purple curves), T_{HIST} ensemble mean (white curve) with shading representing the 95% confidence interval, and T_{obs} (black curves) for comparison. Anomalies are relative to 1970–1999 averages of observations (purple and black curves) and to the POGA average (white curve with shading).

mismatches between the ensemble mean historical simulation and observed GMST exist throughout the instrumental record. During the twentieth century, specifically, the observed GMST features two major warming epochs interrupted by the mid-century big hiatus, unlike the ensemble mean model simulation that shows a nearly continuous warming trend punctuated only by sharp volcanic coolings. Our results show that the IPO is an essential element that makes historical global warming follow a staircase-like evolution. Specifically, the IPO extended the big hiatus by ~10 years, making it both start early and end late compared with the radiatively forced response. Beyond the annual GMST, we identified distinctive fingerprints of the IPO in spatial pattern and seasonal evolution of historical warming. The match of these fingerprints with observations strengthens the case of the IPO as a key pacemaker of global surface temperature change, beyond traditional analyses focused on a single GMST time series.

Large uncertainties exist in estimates of historical radiative forcing and climate sensitivity[22]. To the extent that POGA captures much of the internal variability in GMST, we can infer radiatively forced GMST response as $T_{rad} = T_{obs} - (T_{POGA} - T_{HIST})$, where the term in parentheses represents internal variability induced by tropical Pacific SST (Fig. 4). We emphasize that T_{rad} is independent of the model's radiative forcing and climate sensitivity. While the comparison with observations leaves an impression that HIST overestimates forced GMST change since the 1990s[23] (Fig. 1a), the favourable comparison of T_{rad} and T_{HIST} suggests otherwise. In fact, T_{rad} and T_{HIST} are generally in agreement over the past 120 years including the recent slowdown period, except for a systematic cold bias in T_{HIST} in the 1940s discussed earlier. Volcanic cooling appears overestimated in HIST, but is often compensated in nature by El Niño except for Krakatau (Supplementary Fig. 9). Figure 4 suggests that the HIST simulation captures the forced response quite accurately, including the response to volcanoes. Compared with empirical methods to remove internal variability from observational GMST[24,25], our observation–model hybrid approach considers the timescale dependence—the tropical Pacific effect is 45% larger for decadal than interannual variability (Supplementary Fig. 3)—and event-to-event variations between SST patterns with large anomalies in the central and eastern tropical Pacific (Supplementary Fig. 8).

The world community has come to the consensus of limiting global average temperature change to below 2 °C above pre-industrial levels. Due to substantial internal variability, raw GMST is not a good measure for anthropogenic climate change[26]. We suggest using T_{rad}, which approximates the radiatively forced response better, with the reliable record available since about 1900 (Fig. 4), a time close to pre-industrial conditions. T_{rad} uses models only for estimating internal variability (see Methods for error estimates), and is not subject to the uncertainties in radiative forcing and climate sensitivity. Multimodel pacemaker experiments planned for the Coupled Model Intercomparison Project phase 6 (ref. 27) will provide more information on the consistency of T_{rad} across other models and the utility for monitoring the radiatively forced component of GMST change. Accounting for other climate modes apart from the tropical Pacific effect will further improve estimates of the internal variability effect on GMST.

Methods

Methods, including statements of data availability and any associated accession codes and references, are available in the online version of this paper.

Received 16 March 2016; accepted 20 June 2016; published online 18 July 2016

References

1. Brönnimann, S. Pacemakers of warming. *Nature Geosci.* **8,** 87–89 (2015).
2. Trenberth, K. E. Has there been a hiatus? *Science* **349,** 691–692 (2015).
3. Meehl, G. A., Arblaster, J. M., Fasullo, J. T., Hu, A. X. & Trenberth, K. E. Model-based evidence of deep-ocean heat uptake during surface-temperature hiatus periods. *Nature Clim. Change* **1,** 360–364 (2011).
4. Kosaka, Y. & Xie, S.-P. Recent global-warming hiatus tied to equatorial Pacific surface cooling. *Nature* **501,** 403–407 (2013).
5. England, M. H. *et al*. Recent intensification of wind-driven circulation in the Pacific and the ongoing warming hiatus. *Nature Clim. Change* **4,** 222–227 (2014).
6. Dai, A., Fyfe, J. C., Xie, S.-P. & Dai, X. Decadal modulation of global surface temperature by internal climate variability. *Nature Clim. Change* **5,** 555–559 (2015).
7. Schmidt, G. A., Shindell, D. T. & Tsigaridis, K. Reconciling warming trends. *Nature Geosci.* **7,** 158–160 (2014).
8. Santer, B. D. *et al*. Volcanic contribution to decadal changes in tropospheric temperature. *Nature Geosci.* **7,** 185–189 (2014).
9. Zhang, Y., Wallace, J. M. & Battisti, D. S. ENSO-like interdecadal variability: 1900–93. *J. Clim.* **10,** 1004–1020 (1997).
10. Power, S., Casey, T., Folland, C., Colman, A. V. & Mehta, V. Inter-decadal modulation of the impact of ENSO on Australia. *Clim. Dynam.* **15,** 319–324 (1999).
11. Maher, N., Sen Gupta, A. & England, M. H. Drivers of decadal hiatus periods in the 20th and 21st centuries. *Geophys. Res. Lett.* **41,** 5978–5986 (2014).
12. Fyfe, J. C. *et al*. Making sense of the early-2000s global warming slowdown. *Nature Clim. Change* **6,** 224–228 (2016).
13. Meehl, G. A., Teng, H. & Arblaster, J. M. Climate model simulations of the observed early-2000s hiatus of global warming. *Nature Clim. Change* **4,** 898–902 (2014).
14. Smith, T. M., Reynolds, R. W., Peterson, T .C. & Lawrimore, J. Improvements to NOAA's historical merged land-ocean surface temperature analysis (1880–2006). *J. Clim.* **21,** 2283–2296 (2008).
15. Thompson, D. W. J., Kennedy, J. J., Wallace, J. M. & Jones, P. D. A large discontinuity in the mid-twentieth century in observed global-mean surface temperature. *Nature* **453,** 646–649 (2008).
16. Huang, B. *et al*. Extended reconstructed sea surface temperature version 4 (ERSST.v4). Part I: upgrades and intercomparisons. *J. Clim.* **28,** 911–930 (2015).
17. Brönnimann, S. Early twentieth-century warming. *Nature Geosci.* **2,** 735–736 (2009).
18. Bindoff, N. L. *et al*. in *Climate Change 2013: The Physical Science Basis* (eds Stocker, T. F. *et al*.) 867–952 (IPCC, Cambridge Univ. Press, 2013).
19. Wilcox, L. J., Highwood, E. J. & Dunstone, N. J. The influence of anthropogenic aerosol on multi-decadal variations of historical global climate. *Environ. Res. Lett.* **8,** 024033 (2013).
20. Meehl, G. A., Hu, A. & Santer, B. D. The mid-1970s climate shift in the Pacific and the relative roles of forced versus inherent decadal variability. *J. Clim.* **22,** 780–792 (2009).
21. Thompson, D. M. *et al*. Early twentieth-century warming linked to tropical Pacific wind strength. *Nature Geosci.* **8,** 117–121 (2015).
22. Knutti, R. & Hegerl, G. C. The equilibrium sensitivity of the Earth's temperature to radiation changes. *Nature Geosci.* **1,** 735–743 (2008).

23. Otto, A. *et al*. Energy budget constraints on climate response. *Nature Geosci.* **6,** 413–414 (2013).
24. Thompson, D. W., Wallace, J. M., Jones, P. D. & Kennedy, J. J. Identifying signatures of natural climate variability in time series of global-mean surface temperature: methodology and insights. *J. Clim.* **22,** 6120–6141 (2009).
25. Fyfe, J. C., Gillett, N. P. & Thompson, D. W. J. Comparing variability and trends in observed and modelled global-mean surface temperature. *Geophys. Res. Lett.* **37,** L16802 (2010).
26. Victor, D. G. & Kennel, C. F. Ditch the 2 °C warming goal. *Nature* **514,** 30–31 (2014).
27. Boer, G. J. *et al*. The decadal climate prediction project. *Geosci. Model Dev. Discuss.* http://dx.doi.org/10.5194/gmd-2016-78 (2016).
28. Morice, C. P., Kennedy, J. J., Rayner, N. A. & Jones, P. D. Quantifying uncertainties in global and regional temperature change using an ensemble of observational estimates: the HadCRUT4 data set. *J. Geophys. Res.* **117,** D08101 (2012).
29. Hansen, J., Ruedy, R., Sato, M. & Lo, K. Global surface temperature change. *Rev. Geophys.* **48,** RG4004 (2010).
30. Karl, T. R. *et al*. Possible artifacts of data biases in the recent global surface warming hiatus. *Science* **348,** 1469–1472 (2015).

Acknowledgements

The authors are grateful to the Geophysical Fluid Dynamics Laboratory model developers for making the coupled model version 2.1 available. Y.K. is supported by the Japanese Ministry of Education, Culture, Sports, Science and Technology through Grant-in-Aid for Young Scientists 15H05466 and the Arctic Challenge for Sustainability (ArCS) Project, and by the Japanese Ministry of Environment through the Environment Research and Technology Development Fund 2-1503. S.-P.X. is supported by the US National Science Foundation and National Oceanic and Atmospheric Administration.

Author contributions

Y.K. and S.-P.X. designed the study and wrote the paper. Y.K. performed the model experiments and analysis in consultation with S.-P.X.

Additional information

Supplementary information is available in the online version of the paper. Reprints and permissions information is available online at www.nature.com/reprints. Correspondence and requests for materials should be addressed to Y.K. or S.-P.X.

Competing financial interests

The authors declare no competing financial interests.

Methods

Observational data sets. We used gridded surface temperature data sets of Hadley Centre/Climatic Research Unit (HadCRUT) version 4.4.0.0 (ref. 28) median, US National Aeronautics and Space Administration (NASA) Goddard Institute for Space Studies (GISS) GISTEMP[29] with 250 km smoothing (obtained on 2015-08-03), and US National Oceanic and Atmospheric Administration (NOAA)-National Centers for Environmental Information[30] (hereafter K15). The resolution is 5° × 5° for HadCRUT and K15 and 2° × 2° for GISTEMP. GISTEMP and K15 use NOAA ERSST version 4 over the ocean, which infills missing observations with an empirical method. HadCRUT does not perform such infilling. We do not apply EOF analyses to HadCRUT because of many missing values. SST is compared among ERSST version 3b, version 4 and HadISST version 2.1 (obtained as the 10-member ensemble mean from European Centre for Medium-Range Weather Forecasts (ECMWF) 20th-Century Reanalysis model-only integration (ERA-20CM)[31]).

Model experiments. Methods for HIST and POGA experiments are similar to those of ref. 4. We used the Geophysical Fluid Dynamics Laboratory Coupled Model version 2.1 (ref. 32), at atmospheric resolution of 2° latitude × 2.5° longitude and oceanic resolution of ~1°. The meridional grid spacing reduces from 30° N/S to ~1°/3 at the Equator. 20-member HIST and 10-member POGA were forced commonly with Coupled Model Intercomparison Project phase 5 (CMIP5) historical radiative forcing for 1861–2005 and Representative Concentration Pathway (RCP) 4.5 afterwards. In POGA, we further forced the tropical Pacific variability to follow observations. We used ERSST version 3b, which shows physically consistent multidecadal trends with various independent observations[33]. Here we restored the tropical eastern Pacific SST anomalies by overriding sensible heat flux to the ocean as described in ref. 4. The restoring was applied to 15° S–15° N, the Date Line eastward to the American coast (the inner box of Fig. 2e,h), with 5° buffer zones west, north and south (the outer box), where the restoring linearly decreases to zero. This restoring was applied to model deviation from its climatology (derived as 1920–2005 climatology of HIST) toward observational anomalies relative to the corresponding climatology. Note that we did not change heat flux to the atmosphere, and thus heat budget is not closed. However, the artificial heat for restoring (scaled to global average) is overall weaker than the top-of-the-atmosphere radiation imbalance, and their sum is within ensemble spread of the latter in HIST.

The prescribed tropical Pacific SST anomalies (P) over decadal intervals include internal variability (P_I) and radiatively forced change (P_F). The tropical Pacific effect, defined as the POGA minus HIST difference (Fig. 1c), aims to capture the internal component of GMST change (T_I). The model errors in simulating the forced component of tropical Pacific SST anomalies ($\Delta P_F = P'_F - P_F$) result in errors in estimating the tropical Pacific SST effect relative to the forced change simulated in HIST, as $P = P'_F + (P_I - \Delta P_F)$. Here the prime denotes the model results. The forced change is to first order spatially uniform ($T_F \sim P_F$) while for internal variability, decadal anomalies of GMST scale with those of tropical Pacific SST ($T_I = 0.4P_I$; Supplementary Fig. 3). Decadal GMST anomalies are comparable in magnitude between the internal and forced components, $O(T_I) = O(T_F)$ as in the early 2000s warming slowdown. From these relationships, the forced component of decadal trend in tropical Pacific SST is a fraction of the internal component, $P_F \sim 0.4P_I$. Hence, a 25% model error in P_F yields only a 10% error in estimating internal tropical Pacific variability ($\Delta P_F / P_I \sim 0.1$). This justifies our method to estimate internal GMST variability from POGA results.

We have evaluated the long-term effect of ΔP_F by testing the significance of the tropical SST difference averaged over the SST restoring region between the HIST ensemble mean and ERSST version 3b. We applied the Mann–Kendall test to all combinations with start year from 1896 to 1905 and end year from 1996 to 2005, to avoid strong edge effects. No combination yielded a trend in SST difference significant at $p < 0.1$, indicating that biases in long-term P_F are much smaller than P_I.

While we cannot rule out the possibility that volcanic radiative forcing modulates probability of the IPO[34], IPO phase transitions are not generally attributable to external forcing.

Analyses. We mainly examined 15-year trends of GMST and gridded surface temperature. The 15-year trend window has been used to examine decadal warming modulations in the literature[12,35]. The EOF analysis for Fig. 2 is applied to a domain covering the entire tropics and subtropics (35° S–35° N) plus the North Pacific–North American region (120° E–60° W, 35° N–70° N), where the IPO is influential on surface temperature. The SST restoring region (the outer box of Fig. 2e,h) is excluded. The seasonal EOF analysis for Fig. 3 is performed for zonal average over 35° S–70° N (including the tropical Pacific) and 3-month running mean from January to December. Inclusion of the entire northern extratropics (35° N–70° N) to the spatial EOF domain or exclusion of the SST restoring region from zonal averages for the seasonal EOF does not affect the results. Indeed, correlation coefficients of the leading principal components for these domains with those shown in Figs 2c and 3d exceed 0.97 (spatial EOF) and 0.94 (seasonal EOF) in all of the data sets. The EOF analyses are applied to 15-year trends from 1880–1894 to 2000–2014. The seasonal averages are calculated if data are available at least one month per season. The annual average is calculated if data are available at least one month per season for all of the seasons. Trends were evaluated as the Sen median slope[36], if data are available for over 80% of the trend window. When evaluating $T_{POGA} - T_{HIST}$, the ensemble mean of T_{HIST} is subtracted from each member of T_{POGA}.

We repeated GMST evaluation and EOF analyses by subsampling the model temperature to exclude the grid points of missing observations, and obtained virtually the same results. We also repeated analyses of Figs 1b,c, 2a–c and 3 with 11, 13, 17 and 19-year trends and obtained qualitatively the same results. The correlation coefficient between the leading principal components is lowest for 19-year trends of POGA minus HIST and GISTEMP minus HIST at 0.66 (spatial EOF) and 0.79 (seasonal EOF).

Code availability. The CM2.1 source code can be accessed at http://www.mom-ocean.org. The code for SST restoring can be requested from the corresponding author.

Data availability. HadCRUT, GISTEMP and K15 data sets were obtained at MetOffice web site, GISS web site and NOAA FTP server, respectively. ERSST version 3b and 4 are available at NOAA data repository. HadISST version 2.1 was obtained as part of ERA-20CM at ECMWF web interface. HIST and POGA data are available from the corresponding author on request.

References

31. Hersbach, H. *et al*. *ERA-20CM: A Twentieth Century Atmospheric Model Ensemble* ERA Report Series 16 (ECMWF, 2013); http://www.ecmwf.int/en/elibrary/9870-era-20cm-twentieth-century-atmospheric-model-ensemble
32. Delworth, T. L. *et al*. GFDL's CM2 global coupled climate models. Part I: formulation and simulation characteristics. *J. Clim.* **19,** 643–674 (2006).
33. Tokinaga, H., Xie, S.-P., Deser, C., Kosaka, Y. & Okumura, Y. M. Slowdown of the Walker circulation driven by tropical Indo-Pacific warming. *Nature* **491,** 439–443 (2012).
34. Maher, N., McGregor, S., England, M. H. & Sen Gupta, A. Effects of volcanism on tropical variability. *Geophys. Res. Lett.* **42,** 6024–6033 (2015).
35. Flato, G. *et al*. in *Climate Change 2013: The Physical Science Basis* (eds Stocker, T. F. *et al*.) 741–866 (IPCC, Cambridge Univ. Press, 2013).
36. Sen, P. K. Estimates of the regression coefficient based on Kendall's tau. *J. Am. Stat. Assoc.* **63,** 1379–1389 (1968).